Ag/ZnO hybrid systems studied with scanning tunnelling microscopy-based luminescence spectroscopy

Leandro Pascua,[1] Fernando Stavale,[1,2] Niklas Nilius,[1,3,a)] and Hans-Joachim Freund[1]

[1]*Fritz-Haber-Institut der Max-Planck-Gesellschaft, Faradayweg 4-6, D-14195 Berlin, Germany*
[2]*Centro Brasileiro de Pesquisas Físicas - CBPF/MCTI, Rua Xavier Sigaud 150, 22290-180 Rio de Janeiro, Brazil*
[3]*Institut für Physik, Carl von Ossietzky Universität Oldenburg, D-26111 Oldenburg, Germany*

Coupled metal/oxide systems are prepared by depositing and embedding Ag nanoparticles into crystalline ZnO films grown on Au(111) supports. The morphology and optical properties of the compounds are investigated by topographic imaging and luminescence spectroscopy performed in a scanning tunnelling microscope (STM). The luminescence of bare ZnO is governed by the band-recombination and a Zn-vacancy related peak. After Ag deposition, two additional maxima are detected that are assigned to the in-plane and out-of-plane plasmon in Ag nanoparticles and have energies below and slightly above the oxide band-gap, respectively. Upon coating the particles with additional ZnO, the out-of-plane plasmon redshifts and loses intensity, indicating strong coupling to the oxide electronic system, while the in-plane mode broadens but remains detectable. The original situation can be restored by gently heating the sample, which drives the silver back to the surface. However, the optical response of pristine ZnO is not recovered even after silver evaporation at high temperature. Small discrepancies are explained with changes in the ZnO defect landscape, e.g., due to silver incorporation. Our experiments demonstrate how energy-transfer processes can be investigated in well-defined metal/oxide systems by means of STM-based spectroscopic techniques. © 2016 AIP Publishing LLC.
[http://dx.doi.org/10.1063/1.4943070]

I. INTRODUCTION

ZnO is an archetypical semiconducting oxide with a direct band gap in the ultraviolet (3.4 eV) and a large exciton binding energy of 60 meV.[1] Its unique optical response, in combination with favorable chemical properties, makes ZnO a promising material for applications in photochemistry and photocatalysis. In fact, a huge number of studies has been carried out on ZnO and its derivatives,[2,3] only topped by TiO_2 that features similar optoelectronic properties.[4,5] The research activities on ZnO largely focus on an efficient generation of photo-carriers as required for photochemical reactions. Two strategies have been followed to enhance the excitation cross-section of electron-hole pairs that is tuning the ZnO gap size and adding photosensitizers to the surface.[6] Band-gap engineering typically relies on the insertion of impurities that produce new gap states and therefore enhance the visible-light absorption.[7] Promising gap-reducing species are aliovalent dopants placed on Zn^{2+} sites, e.g., Al,[8] Ga,[9] or Mg,[10] as well as anionic impurities such as nitrogen.[11] A main drawback of the approach is the poor spatial overlap of defect states in the gap, causing the photo-generated carriers to become trapped below the surface.

Also photosensitizers enhance the absorption and scattering of photons, hence the interaction between ZnO and the incoming radiation. As the photochemical step still occurs in the oxide and not in the sensitizer, energy exchange with the

ZnO support remains mandatory. Sensitizers that are known to augment the coupling to light are Dye molecules[12] and plasmonic particles.[13–15] Whereas single-electron transitions are responsible for photon absorption in the former case, collective excitations with large oscillator strength interact with the photon field in the latter. Plasmon-mediated sensitizing follows two principles. If the plasmon energy is smaller than the ZnO band gap, as in the case of Au and Cu particles, hot electrons arising from Landau damping of the collective modes are injected into the oxide bands. Conversely, direct plasmon-exciton coupling, Förster energy transfer, or re-absorption of scattered photons becomes important if the plasmon energy exceeds the gap width. Note that functionalization of ZnO with plasmonic particles is of relevance not only for photochemistry but also for the fabrication of thin-film solar cells and supports for surface-enhanced Raman spectroscopy.[16,17]

Preparation and characterization of metal/oxide hybrid systems have been extensively reported in the literature.[1] In most examples, ZnO nanostructures, e.g., rods, pillars, or spheres, are functionalized either with silver[18,19] or gold particles.[20,21] Their density and geometry are typically derived from electron-microscopy studies, while absorption and photoluminescence experiments are used to explore their electromagnetic coupling to the oxide support. Silver deposition was found to enhance the UV luminescence of ZnO, indicating an energy transfer from metal plasmons to oxide excitons.[22–24] As the energy of the dipolar Ag plasmon is smaller than the ZnO gap, quadruple modes were made responsible

a)Author to whom correspondence should be addressed. Electronic mail: niklas.nilius@uni-oldenburg.de

for the UV enhancement.[19] Surprisingly, a higher luminescence yield was also reported for Au-functionalized ZnO, although the plasmon energy is smaller than the gap size in this case.[21] The finding was explained with a transfer of photo-generated carriers from the particles to the oxide conduction band, followed by an electron backflow from excited ZnO defect states towards the Fermi level of gold. As a result, both hot electrons and holes accumulate in the oxide bands, producing the observed UV radiation.[10]

Most metal/ZnO hybrid systems in the literature were prepared by wet-chemical methods, such as metal-organic epitaxy,[25] solvothermal[26] and electrochemical deposition; techniques that sometimes suffer from sample contamination with parasitic agents. Moreover, fabrication and characterization of the systems were often realized in different setups, involving a transport through air. To overcome these drawbacks, we have vapour-deposited Ag nanoparticles onto atomically flat ZnO/Au(111) films in the present study. Morphology and optical properties of the hybrid systems were probed in a single vacuum chamber by scanning tunnelling microscopy (STM) and luminescence spectroscopy. Our experiments revealed a small coupling between Ag plasmons and ZnO excitons that could be enhanced by embedding the particles into the oxide matrix.

II. EXPERIMENTAL

Experiments are carried out in an ultra-high vacuum chamber (2×10^{-10} mbar), equipped with a liquid-nitrogen cooled STM and standard facilities for sample preparation and analysis. Our microscope is specifically designed to collect photons from the tip-sample junction.[27] For this purpose, the STM head is placed inside a parabolic mirror that collects the photons and directs them out of the vacuum into a 150 lines/mm-grating spectrograph coupled to a CCD detector. ZnO films of approximately 25 ML thickness are prepared by sublimating ZnO pellets in 5×10^{-5} mbar of O_2 onto a sputtered and annealed Au(111) single crystal.[11]

Annealing to 700 K in the same O_2 ambience triggers crystallization of the film and results in a sharp, hexagonal electron-diffraction pattern that is typical for a ZnO(0001)-type termination (Fig. 1(a)). A high surface quality is revealed from STM images, showing wide and flat terraces delimited by straight edges running along the symmetry directions of the wurtzite lattice. A finite surface roughness is explained with a disordered hydrogen over-layer that develops spontaneously in order to compensate for the intrinsic polarity of ZnO(0001). Hydrogenation is hereby the expected response for the O-terminated surface, which develops on electronegative Au(111) that tends to stabilize cationic Zn at the interface. The silver was evaporated from a Knudsen cell onto freshly prepared oxide films at 300 K. Its nominal thickness was calibrated by Ag evaporation onto bare Au(111), where it grows in a layer-by-layer fashion and enables direct determination of the surface coverage by STM. To enhance the Ag/ZnO coupling in some cases, the metal particles were coated with ZnO-layers of varying thickness. The Ag/ZnO morphology was further modified by annealing the samples to different temperatures, as specified in the text.

III. RESULTS AND DISCUSSION

A. Growth of Ag particles on ZnO films

Figure 1 displays a growth sequence of silver on a 25 ML-thick ZnO film performed at 300 K. At the lowest exposure (nominally 1.5 ML), nearly hemispherical particles of approximately (1.5 ± 0.5) nm height and 3–5 nm diameter develop on the surface. The lateral dimensions have been corrected for tip-convolution effects by comparing apparent and nominal Ag coverages. The particles homogenously cover the oxide surface with an average density of 5×10^{12} cm^{-2}. After doubling the Ag exposure to 3 ML, the particles increase to (2.5 ± 1.0) nm height and 6–8 nm diameter, while their density decreases to 2.5×10^{12} cm^{-2}.
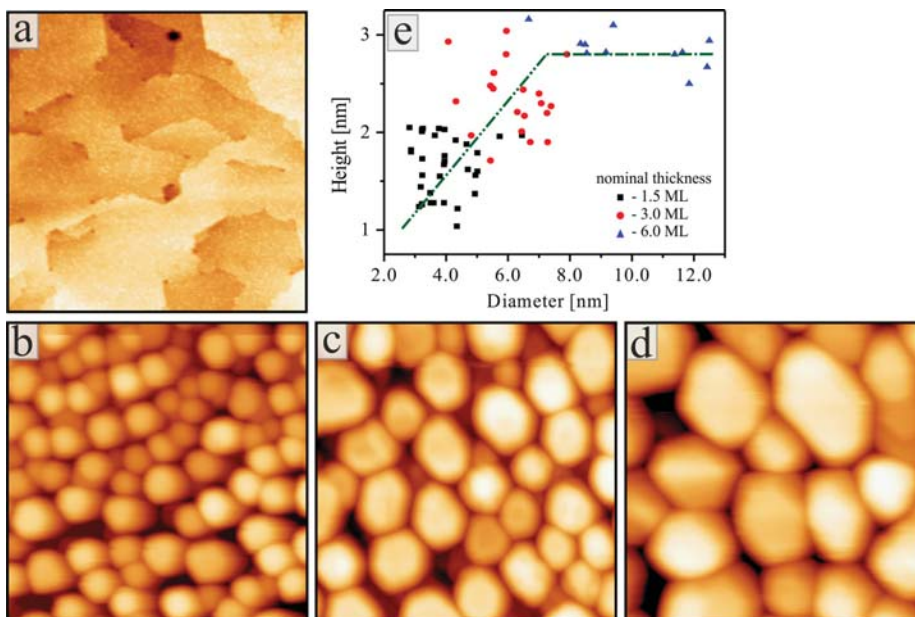

FIG. 1. (a) STM topographic image of 25 ML bare ZnO grown on Au(111) (200×200 nm^2, $U_s = 3.0$ V). Similar film after depositing nominally (b) 1.5, (c) 3.0, and (d) 6 ML silver at room temperature (35×35 nm^2, 3.0 V). (e) Height and diameter of Ag particles as deduced for the three coverages. The particle aspect ratio was determined to 0.4 in the growth regime; the coalescence regime was reached at about 8 nm particle diameter.

Simultaneously, some particles develop distinct hexagonal shapes, indicating their crystalline nature.[28] A further rise of the Ag exposure to 6 ML leads to crystallites with (3.5 ± 1.0) nm height, 8–12 nm width, and prominent hexagonal top facets. Conversely, the particle density drops to 1×10^{12} cm^{-2} due to coalescence of adjacent deposits. Following the literature,[29,30] we assign the Ag particles to fcc-nanocrystals, delimited by (111) top facets and alternating (111) and (100) side planes. The resulting geometry is compatible with the hexagonal particle appearance in STM, but also with the Wulff model that connects equilibrium shape and free-energies of the respective silver facets.[31] Compared to other ad-metals on ZnO/Au(111), the silver forms loosely packed particle arrays, while Au and Cr ensembles are denser by a factor of 1.4 and 2.2, respectively.[32,33] Accordingly, mean particle sizes decrease when moving from Ag to Au and Cr deposits. This trend reflects the chemical inertness and high mobility of silver that is unable to form true chemical bonds with the hydroxylated ZnO surface.

The STM images in Fig. 2 show the evolution of the Ag/ZnO morphology if the particles are covered with a ZnO ad-layer. The layer thickness hereby increases from 2 ML in (a) to 10 ML in (b). In both cases, the Ag particles remain distinguishable through the ZnO coating and, apart from a blurred appearance, change neither their density nor size. Figure 2(c) shows STM data of an Ag ensemble after coating with 10 ML ZnO and vacuum annealing to 500 K. In the annealing step, the silver seems to move to the surface again, as suggested by the reappearance of sharp and pronounced particle edges. Moreover, strong Ostwald ripening occurs,
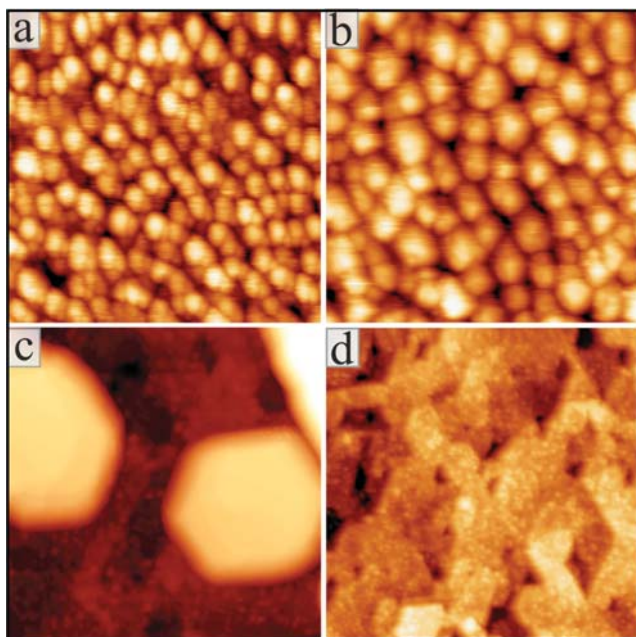

FIG. 2. STM images of 3 ML silver on ZnO coated with an extra ZnO layer of (a) 2 ML and (b) 10 ML thickness (75×75 nm^2, $U_s = 3.0$ V). Despite the coating, the particles remain discernible. Similar sample as in (b) but annealed to (c) 500 K and (d) 700 K after the coating (150×150 nm^2, $U_s = 3.0$ V). Whereas coalescence is the dominating process in (c), the silver evaporates from the surface at 700 K.

resulting in particles with flat, hexagonal top facets and diameters as large as 20–50 nm. Conversely, the particle density reduces to $\sim 2 \times 10^{10}$ cm^{-2}. Further heating to 700 K causes the silver to desorb, and the pristine ZnO surface reappears in the STM images (Fig. 2(d)). Parts of the silver may also migrate into the oxide film, a scenario that gets supported by the optical data discussed in Sec. III C.

B. Optical properties of the Ag/ZnO hybrid system

The optical response of the Ag/ZnO system was studied with STM luminescence spectroscopy.[34,35] The measurements were performed by electron injection from the STM tip into a pre-characterized surface region of 100×100 nm^2. To ensure its morphological integrity during acquisition, the region of interest was scanned before and after each spectral run. Emission spectra of acceptable signal-to-noise ratio have been taken at 150 V excitation bias and 5 nA electron current; the photon signal was accumulated for 600 s at the CCD detector. Note that no luminescence signal could be measured below 50 eV-electron energy, and single-particle spectroscopy was thus impossible.

Figure 3 depicts characteristic STM luminescence spectra taken at each step of our experimental series, i.e., on the bare ZnO surface, after depositing and embedding the Ag particles, and after annealing. Our conclusions are based on several of such runs, all of them showing similar although not identical optical signatures. The black curve at the bottom of Fig. 3 displays the emission response of bare ZnO and largely agrees with the results of earlier publications.[36] The spectrum is governed by a sharp peak at 373 nm (3.3 eV), assigned to the band recombination in ZnO. The excitonic nature of the transition is not resolved at the temperature of the measurement. The second peak at 535 nm (2.3 eV) relates to a defect-mediated emission channel, arising from radiative electron decay via Zn vacancy states in the oxide band gap.[36] Zn vacancies were identified as the main defect-type in our ZnO films, as they provide charges for compensating the excess electrons in the intrinsically n-doped material.[37] According to theory, the n-type character originates from hydrogen donors that are abundant in the wurtzite lattice[38] and cannot be eliminated even in ultrahigh vacuum systems. The 535 nm-peak is therefore intrinsic to our films and all attempts to suppress this emission failed.[36] Finally, the faint shoulder at 730 nm (1.7 eV) is assigned to a small number of O defects in the ZnO lattice,[39] but plays no role in further discussions.

Deposition of 3 ML silver gives rise to several changes in the spectra (Fig. 3, 2nd curve). First, the ZnO-related peaks loose about 50% of their intensity, readily explained with the Ag particles that cap the oxide film and block the tip electrons. In addition, two new maxima emerge in the spectra, a low-wavelength peak at 320 nm (3.85 eV, FWHM 430 meV) and a broader band at 600 nm (2.1 eV, FWHM 590 meV) (Table I). The peaks are directly related to the Ag deposits and intensify with increasing Ag exposure. They represent the optical fingerprints of silver plasmon modes, as discussed below. When covering the particle ensemble with 10 ML ZnO, the plasmon-related peaks smear out and shift
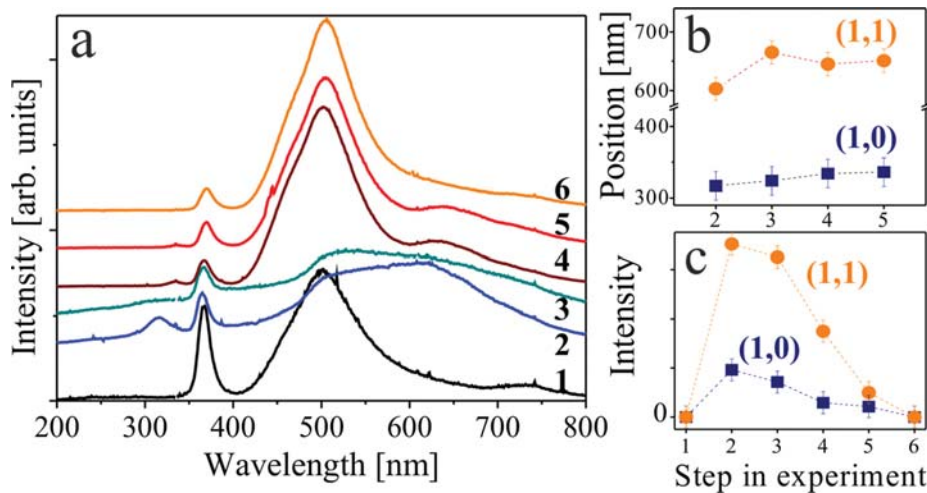
FIG. 3. (a) STM luminescence spectra of bare ZnO (1), after 3 ML Ag exposure (2), after coating with 10 ML ZnO (3), and after annealing to 400, 550 and 700 K (4–6). The panels on the right show the evolution of (b) the position and (c) the intensity of (1,0) and (1,1) plasmon peaks of silver after subtracting the ZnO contribution.

to longer wavelengths (3rd curve). Interestingly, the ZnO emission does not recover at this point, most likely because the ad-layer has insufficient crystallographic quality to enable radiative exciton decay. The situation changes substantially after annealing the sample to temperatures between 400 and 700 K. After a first heating step (4th curve), the Ag plasmon peaks sharpen again, indicative for the restoration of a homogenous dielectric environment around the deposits. The peaks also experience a red-shift, in which the low- and high-wavelength features move to 340 nm (3.65 eV) and 640 nm (1.9 eV), respectively. The new positions remain approximately constant during further annealing; but reduce their intensity to 50% at 550 K and finally to zero at 700 K. However, the ZnO bands are not fully restored even after silver removal. While the band recombination peak remains at half of its initial height, the Zn-defect emission intensifies, suggesting an increasing number of Zn-defects after the procedure. We will discuss possible reasons for this behavior in Sec. III C.

C. Interpretation of the optical data

Growing an Ag particle ensemble onto the oxide film adds a plasmonic component to the optical spectra that only featured ZnO band-recombination and defect-emission before. The relevant plasmon energies are estimated from the energy-dependent polarizability $\alpha(\omega)$ of an Ag spheroid in a dielectric matrix[40]

$$\alpha(\omega) \propto \frac{\varepsilon(\omega) - \varepsilon_m}{3\varepsilon_m + 3L_{\perp,\parallel}[\varepsilon(\omega) - \varepsilon_m]}. \quad (1)$$

TABLE I. Experimental Ag plasmon peaks as determined from STM luminescence spectra taken after the indicated preparation steps.

Preparation step	Position of (1,0) plasmon (nm)	Position of (1,1) plasmon (nm)
Silver deposition	320	600
ZnO-coating	325	668
400 K annealing	340	640
550 K annealing	340	650

Here, $\varepsilon(\omega)$ is the experimentally determined silver dielectric function,[41] and ε_m describes the dielectric surrounding of the particle, being composed of the ZnO film below ($\varepsilon_{m'} = 3.7$)[42] and the vacuum above ($\varepsilon_{m''} = 1$). Particle shapes, as derived from experimental aspect ratios, enter the formula via the depolarization factors L. Whereas $L_{\perp}$ stands for the vertical polarizability of the deposits and controls the out-of-plane (1,0) plasmon, $L_{\parallel}$ accounts for the horizontal polarizability, hence for the in-plane (1,1) mode. The different depolarization components add up to one, according to $2(L_{\parallel}) + L_{\perp} = 1$. The imaginary part of the polarizability now determines the plasmon-related absorption cross section of the deposits and, due to the resonant nature of plasmon excitations, also their emission response.[40] For non-embedded, prolate Ag particles with an aspect ratio of 0.4, the two plasmon modes are calculated to be at $\hbar\omega_{1,0} = 3.8$ eV and $\hbar\omega_{1,1} = 2.3$ eV. Both values agree well with the emission peaks at 3.85 and 2.1 eV, observed after Ag deposition onto ZnO, and are consequently assigned to the vertical and horizontal plasmon modes in the Ag deposits. The small discrepancy is attributed to the disregard of particle-particle interactions that are constructive for in-plane modes, lowering their energy, but destructive for out-of-plane oscillations. Our interpretation is in line with literature data, acquired for Ag particles either precipitated onto ZnO nanorods or embedded into ZnO matrices.[24] In both cases, prominent luminescence peaks were observed at 2.1 eV and explained with the decay of (1,1) plasmons in the ad-metal. The high-lying (1,0) mode has not been detected in that study, most likely due to its energy above the fundamental ZnO band gap and the associated damping.

In the course of the experiment, the Ag particles have been coated with 10 ML ZnO in order to increase the efficiency of metal/oxide coupling. As a result, the experimental plasmon modes broadened and shifted towards higher wavelength, both trends being compatible with a larger influence of the dielectric matrix on the collective excitations (Fig. 3, 3rd curve). To simulate this effect, we first consider as-grown Ag particles that only share a ZnO interface at the bottom and are exposed to vacuum otherwise. This situation is described with a dielectric constant averaged over 35%
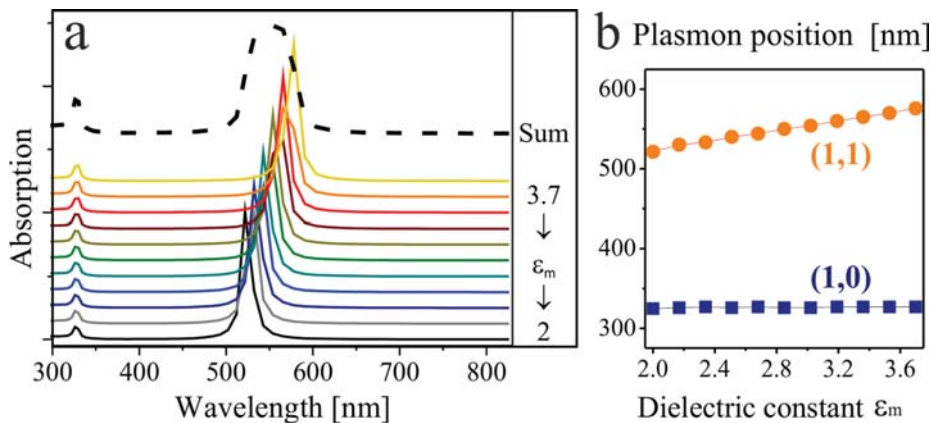
FIG. 4. (a) Calculated absorption spectra for prolate Ag particles embedded in different dielectric environments. Whereas $\varepsilon_m = 2$ corresponds to a surface-bound deposit, $\varepsilon_m = 3.7$ reflects a particle that is fully embedded in ZnO. (b) Evolution of the (1,0) and (1,1) plasmon energy as a function of the dielectric environment.

ZnO and 65% vacuum, yielding an effective ε_m of 2. Upon adding ZnO on top, the vacuum gets replaced by an oxide layer, and the effective dielectric constant increases towards the bulk ZnO value of 3.7. However, the coating discussed here is well below the typical penetration depth of light, and only an incomplete dielectric response of the ZnO film can be expected.[40] Still, the energy shift of the plasmon due to ZnO embedding is evident, both in experiment and simulation (Figs. 3(b) and 4(a)). With increasing ε_m, the calculated in-plane resonance $\hbar\omega_{1,1}$ redshifts from 2.3 to 2.1 eV, following the experimental trend. Simultaneously, the peak broadens, as the thickness of the ZnO cap is not homogenous and different Ag deposits experience slightly different dielectric environments. We have reproduced this effect by summing up the particles optical response calculated for different ε_m values (Fig. 4(a), dashed line).

Markedly, the (1,0) mode experiences not only a broadening but also an intensity reduction after coating with additional ZnO. We take this finding as experimental evidence for an energy transfer between Ag plasmons and electron-hole pairs in the oxide film.[43] Unfortunately, this energy exchange does not result in a higher ZnO emission yield, although such an effect has been anticipated from the role of Ag particles as optical sensitizers.[22–24] We believe that the low crystallographic quality of our ZnO ad-layer is responsible for the missing enhancement. Apparently, the as-grown layer offers too many non-radiative recombination channels to enable a plasmon-mediated increase of the luminescence.

In order to address this point, we have gently annealed the Ag/ZnO hybrid systems in the last step of our experiment.

The annealing partly recovers the plasmonic response of the Ag ensemble with respect to the situation prior to ZnO coating. Both, the (1,0) and (1,1) resonances reappear in the spectra as relatively sharp lines, but are red-shifted by ~0.2 eV to 3.65 and 1.9 eV, respectively (Table I). The reason for this shift can be rationalized with the help of the STM data. Upon annealing, the silver floats to the surface, and the extra ZnO merges with the original film and partly encloses the deposits. In addition, the overall particle size increases, and the aspect ratio gets smaller (flatter particles, Fig. 2(c)). Both, the changes in particle geometry and dielectric environment govern the observed shift of the plasmon resonance. Whereas the particle flattening controls the in-plane resonance and governs its shifts to higher wavelength (Fig. 5),[44] the dielectric environment mostly acts on the out-of-plane mode, producing a slight redshift as the particle sinks into the oxide film. The sharpening of the plasmon peaks finally reflects the higher structural homogeneity of the system after thermal treatment.

With rising temperature, another trend dominates the spectral response that is the loss of plasmon intensity due to the silver evaporation from the surface. While the peaks are still discernable at 550 K annealing, only the ZnO emission remains visible beyond 700 K. However, this ZnO emission is not identical to the one observed prior to Ag evaporation (Fig. 3). In fact, the band-recombination peak at 373 nm has
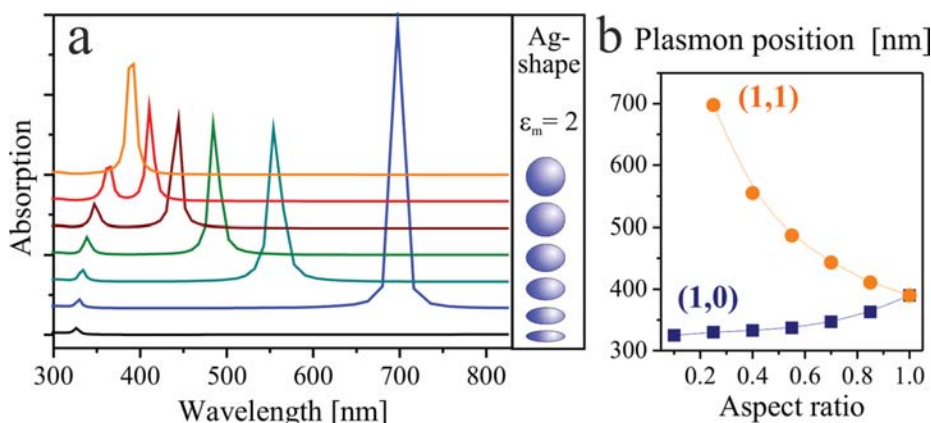

FIG. 5. (a) Calculated absorption spectra of surface-bound Ag particles of different shapes. (b) Evolution of the (1,0) and (1,1) plasmon modes as a function of the particle aspect ratio.

lost more than half of its initial height, while the Zn-vacancy peak has slightly gained intensity. The first trend is tentatively explained with a loss of crystallographic quality, caused by the addition of silver and amorphous ZnO to the surface. The second trend rather points to the development of extra Zn defects in the lattice, probably as a means to balance a higher electron count in the system. Two sources for excess electrons are conceivable. Traces of silver may have entered interstitial sites of the wurtzite lattice, acting as electron donors and stimulating the formation of compensating Zn defects.[45,46] Also, the metallic Ag particles on-top or inside the ZnO may serve as electron reservoirs, suitable for charge exchange with acceptor states in the ZnO band gap. We note that independent of the Ag exposure, an increase of the Zn-defect peak has been revealed after annealing ZnO thin films in oxygen excess.[36]

IV. CONCLUSIONS

In order to study energy-transfer processes between plasmonic and excitonic systems, we have prepared Ag particle ensembles on crystalline and atomically flat ZnO films. As long as the nanoparticles reside on the surface, the coupling between both systems is negligible, and the luminescence spectra are characterized by the superposition of two plasmons ($\hbar\omega_{1,0}$ and $\hbar\omega_{1,1}$) and two ZnO-related peaks. The metal/oxide interaction increases upon embedding the Ag particles into a ZnO ad-layer. While the plasmon modes broaden and red-shift due to the altered dielectric environment, the ZnO emission loses intensity. This is in contrast to the expected luminescence enhancement, ascribed to plasmon-exciton energy-transfer. We explain the absence of a clear coupling signature with the low quality of the Ag/ZnO interface and the abundance of structural defects in the ZnO ad-layer. Moreover, the oxide cover is probably too thin to allow for an efficient absorption of the plasmon energy. Attempts to improve the structural quality of the system failed, as silver was found to float to the surface upon annealing, causing the metal/oxide coupling strength to decrease again. The dilemma might be solved by precipitating ZnO ad-layers that are thick enough to keep the particles embedded even after thermal treatment. However, as the Ag particles reside deep below the surface in this case, corresponding experiments should be performed with classical optical techniques instead of surface-sensitive STM-approaches.

ACKNOWLEDGMENTS

[1]Ü. Özgür, Y. I. Alivov, C. Liu, A. Teke, M. A. Reshchikov, S. Doğan, V. Avrutin, S.-J. Cho, and H. Morkoç, J. Appl. Phys. **98**, 041301 (2005).

[2]U. Diebold, S. C. Li, and M. Schmid, Annu. Rev. Phys. Chem. **61**, 129 (2010).

[3]C. Wöll, Prog. Surf. Sci. **82**, 55 (2007).

[4]M. D. Hernandez-Alonso, F. Fresno, S. Suarez, and J. M. Coronado, Energy Environ. Sci. **2**, 1231 (2009).

[5]S. Rehman, R. Ullah, and A. M. Butt, J. Hazard. Mater. **170**, 560 (2009).

[6]H. Rensmo, K. Keis, H. Lindström, S. Södergren, A. Solbrand, A. Hagfeldt, S.-E. Lindquist, L. N. Wang, and M. Muhammed, J. Phys. Chem. B **101**, 2598 (1997).

[7]R. Janisch, P. Gopal, and N. Spaldin, J. Phys.: Condens. Matter **17**, R657 (2005).

[8]I. Valenti, S. Benedetti, A. di Bona, V. Lollobrigida, A. Perucchi, P. Di Pietro, S. Lupi, S. Valeri, and P. Torelli, J. Appl. Phys. **118**, 165304 (2015).

[9]B. K. Meyer, H. Alves, D. Hofmann, W. Kriegseis, D. Forster, F. Bertram, J. Christen, A. Hoffmann, M. Straßburg, and M. Dworzak, Phys. Status Solidi **241**, 231 (2004).

[10]F. K. Shan, B. I. Kim, G. X. Liu, Z. F. Liu, J. Y. Sohn, W. J. Lee, B. C. Shin, and Y. S. Yu, J. Appl. Phys. **95**, 4772 (2004).

[11]F. Stavale, L. Pascua, N. Nilius, and H.-J. Freund, J. Phys. Chem. C **118**, 13693 (2014).

[12]J.-J. Wu, G.-R. Chen, and H.-H. Yang, Appl. Phys. Lett. **90**, 213109 (2007).

[13]C. W. Lai, J. An, and H. C. Ong, Appl. Phys. Lett. **86**, 251105 (2005).

[14]P. Cheng, D. Li, and Z. Yuan, Appl. Phys. Lett. **92**, 041119 (2008).

[15]J. M. Lin, H. Y. Lin, Y. Hsia, and C. L. Chengl, Nanotechnology **17**, 4391 (2006).

[16]F.-J. Haug, T. Söderström, O. Cubero, V. Terrazzoni-Daudrix, and C. Ballif, J. Appl. Phys. **104**, 064509 (2008).

[17]G. Shan, L. Xu, G. Wang, and Y. Liu, J. Phys. Chem. C **111**, 3290 (2007).

[18]D. C. Mayo, C. E. Marvinney, E. S. Bililign, J. R. McBride, R. R. Mu, and R. F. Haglund, Thin Solid Films **553**, 132 (2014).

[19]Y. Zang, X. He, J. Li, J. Yin, K. Li, C. Yue, Z. Wu, S. Wu, and J. Kang, Nanoscale **5**, 574 (2013).

[20]D. Zhang, H. Ushita, P. Wang, C. Park, R. Murakami, S. Yang, and X. Song, Appl. Phys. Lett. **103**, 093114 (2013).

[21]S. Park, Y. Mun, S. Ana, W. In Lee, and C. Lee, J. Lumin. **147**, 5 (2014).

[22]L. Su, N. Qin, W. Xie, J. Fu, and D. Bao, J. Appl. Phys. **116**, 063108 (2014).

[23]J. Jiménez, S. Lysenko, and H. Liu, J. Appl. Phys. **104**, 054313 (2008).

[24]R. K. Roy, S. Bandyopadhyaya, and A. K. Pal, Eur. Phys. J. B **39**, 491 (2004).

[25]J. Y. Park, Y. S. Yun, Y. S. Hong, H. Oh, J. J. Kim, and S. S. Kim, Appl. Phys. Lett. **87**, 123108 (2005).

[26]Y. Zhang, H. B. Jia, R. M. Wang, C. P. Chen, X. H. Luo, D. P. Yu, and C. J. Lee, Appl. Phys. Lett. **83**, 4631 (2003).

[27]H.-J. Freund, N. Nilius, T. Risse, S. Schauermann, and T. Schmidt, ChemPhysChem **12**, 79 (2011).

[28]S. Benedetti, P. Myrach, A. di Bona, S. Valeri, N. Nilius, and H.-J. Freund, Phys. Rev. B **83**, 125423 (2011).

[29]K. H. Hansen, T. Worren, S. Stempel, E. Lægsgaard, M. Bäumer, H. J. Freund, F. Besenbacher, and I. Stensgaard, Phys. Rev. Lett. **83**, 4120 (1999).

[30]F. Silly and M. R. Castell, Phys. Rev. Lett. **96**, 086104 (2006); F. Silly, A. C. Powell, M. G. Martin, and M. R. Castell, Phys. Rev. B **72**, 165403 (2005).

[31]G. Wulff, Z. Krystallogr. **34**, 449 (1901).

[32]L. Pascua, "Exploring the luminescence characteristics of zinc oxide thin films: The role of defects, impurities and metal ad-particles," Ph.D. dissertation (Freie Universität Berlin, 2015).

[33]B. Kumari, B. S. Sharma, V. R. Satsangi, S. Dass, and R. Shrivastav, J. Appl. Electrochem. **45**, 299 (2015).

[34]N. Nilius, N. Ernst, and H.-J. Freund, Phys. Rev. Lett. **84**, 3994 (2000).

[35]E. M. Likovich, R. Jaramillo, K. J. Russell, S. Ramanathan, and V. Narayanamurti, Appl. Phys. Lett. **99**, 151910 (2011).

[36]F. Stavale, N. Nilius, and H.-J. Freund, J. Phys. Chem. Lett. **4**, 3972 (2013).

[37]A. Janotti and C. G. Van de Walle, Phys. Rev. B **76**, 165202 (2007).

[38]C. G. Van de Walle, Phys. Rev. Lett. **85**, 1012 (2000).

[39]K. E. Knutsen, A. Galeckas, A. Zubiaga, F. Tuomisto, G. C. Farlow, B. G. Svensson, and A. Y. Kuznetsov, Phys. Rev. B **86**, 121203 (2012).

[40]U. Kreibig and W. Vollmer, *Optical Properties of Metal Clusters* (Springer, Berlin, 1995), Vol. 25.

[41]E. D. Palik, *Handbook of Optical Constants of Solids* (Academic, Orlando, 1985).

[42]T. Hanada, "Basic properties of ZnO, GaN, and related materials," in *Oxide and Nitride Semiconductors*, Springer series Advances in Materials Research Vol. 12 (Springer, Berlin, Heidelberg, 2009).

[43]N. Nilius, N. Ernst, and H.-J. Freund, Chem. Phys. Lett. **349**, 351 (2001).

[44]T. Wenzel, J. Bosbach, F. Stietz, and F. Träger, Surf. Sci. **432**, 257 (1999).

[45]R. Schlesinger, Y. Xu, O. T. Hofmann, S. Winkler, J. Frisch, J. Niederhausen, A. Vollmer, S. Blumstengel, F. Henneberger, and P. Rinke, Phys. Rev. B **87**, 155311 (2013).

[46]T. Pauporté, O. Lupan, J. Zhang, T. Tugsuz, I. Ciofini, F. Labat, and B. Viana, ACS Appl. Mater. Interfaces **7**, 11871–11880 (2015).